




Research Article

Anticorectal Cancer Activity of Bilobalide in Patient-Derived Colorectal Cancer Organoids and AOM/DSS Mouse Model

Heng Zhang,¹ Shuhua Fang,² Faisal Raza ,³ Nengqi Cao,¹ Xingchao Fang,¹ Xu Lu,¹ Ran Li,⁴ Feng Shi,⁵ Deqiang Wang ,⁵ and Min Xu ^{5,6}

¹Department of General Surgery, Nanjing Lishui District People's Hospital, Zhongda Hospital Lishui Branch, Affiliated Hospital of Southeast University, Nanjing 211200, China

²Department of Pharmacy, Nanjing Lishui District People's Hospital, Zhongda Hospital Lishui Branch, Affiliated Hospital of Southeast University, Nanjing 211200, China

³School of Pharmacy, Shanghai Jiao Tong University, No. 800, Dongchuan Road, Shanghai 200240, China

⁴College of Pharmacy, Jiangsu University, Zhenjiang 212001, China

⁵Institute of Digestive Diseases, Jiangsu University, Zhenjiang 212001, China

⁶Department of Gastroenterology, Affiliated Hospital of Jiangsu University, Zhenjiang 212001, China

Correspondence should be addressed to Faisal Raza; faisalraza@sju.edu.cn, Deqiang Wang; deqiang_wang@aliyun.com, and Min Xu; peterxu1974@163.com

Received 17 April 2023; Revised 18 January 2024; Accepted 19 March 2024; Published 4 April 2024

Academic Editor: Mohammad Reza Kalhori

Copyright © 2024 Heng Zhang et al. This is an open access article distributed under the Creative Commons Attribution License, which permits unrestricted use, distribution, and reproduction in any medium, provided the original work is properly cited.

Bilobalide has shown strong anti-inflammatory activity. Colorectal cancer (CRC) is closely associated with inflammation. However, no studies have reported on the use of bilobalide for treating CRC. This study aims to evaluate the effect of bilobalide on CRC prevention. Enzyme-linked immunosorbent assay (ELISA), quantitative real-time polymerase chain reaction (RT-qPCR), Western blotting, and immunofluorescence showed that bilobalide significantly inhibits the M2 polarization of macrophages dependent on phorbol 12-myristate 13-acetate (PMA) and interleukin-4 (IL-4). Analysis of signaling pathways showed that the phosphorylation of extracellular signal-regulated kinase (ERK), c-Jun N-terminal kinase (JNK), and signal transducer and activator of transcription 3 (STAT3) was regulated. In particular, human CRC organoids were established. Western blotting, terminal deoxynucleotidyl transferase biotin-dUTP nick end labeling (TUNEL), and analysis of cell viability and morphology further supported the hypothesis that the anti-CRC effects of bilobalide could be explained by its ability to suppress M2 macrophage polarization and promote M1 transformation. C57BL/6 mice treated with azoxymethane (AOM)/dextran sodium sulfate (DSS) were divided into three groups, i.e., control, AOM/DSS, low (2.5 mg/kg), and high (5 mg/kg). High-dose bilobalide markedly inhibited the progression of CRC, as evidenced by the increased body weight, decrease in disease activity index (DAI) death rate, and alleviation of colon length reduction and tumorigenesis. According to the *in vivo* results, reduced levels of inflammatory cytokines in the serum included tumor necrosis factor (TNF- α), IL-6, IL-1 β , and IL-10. Bilobalide reduced oxidative stress indices, lipid peroxide (LPO), and malondialdehyde (MDA) and increased reduced glutathione (GSH). In addition, the expression of proliferating cell nuclear antigen (PCNA), Ki67, cellular Myc (c-Myc), and CD206 was downregulated in the drug-treated groups, as confirmed by the immunohistochemical staining. Collectively, these results indicated that bilobalide administration improve experimental CRC by inhibiting M2 macrophage polarization and oxidative stress. Thus, bilobalide may prevent CRC and serve as a potential therapeutic target for CRC.

1. Introduction

Colorectal cancer (CRC) is the third most common cancer in men and the second most common cancer in women worldwide [1, 2]. Ulcerative colitis, familial adenomatous polyposis, and hereditary nonpolyposis colon cancer syndrome are the three highest risk factors for developing CRC [1]. Increasing evidence has shown that people with inflammatory bowel diseases, such as ulcerative colitis and Crohn's disease, have a 5- to 10-fold increased risk of developing CRC [3, 4]. Numerous studies have shown that persistent inflammation promotes tumor formation and malignant progression [5]. Moreover, a large body of research has focused on the complex inflammatory microenvironment and indicated that targeting inflammation may be an effective strategy for preventing human CRC in patients with inflammatory bowel disease [4, 6, 7].

Tumor-associated macrophages (TAMs) are one of the most important immune cells in the tumor microenvironment that play a key role in tumor development. Polarization of TAMs into a tumor-suppressive M1 or a tumor-promoting M2 phenotype is a fundamental event that is closely associated with tumor prognosis. In most cancer cases, TAMs stimulate colon cancer cell growth, invasion, metastasis, and immune evasion and are usually present in the M2 polarization state in the tumor microenvironment [8–10]. CD206, arginase-1 (Arg-1), interleukin-4 (IL-4), IL-10, and transforming growth factor- β are the main markers for the M2 phenotype, whereas the M1 markers include CD11b, inducible nitric oxide synthase (iNOS), IL-12, IL-6, and tumor necrosis factor- α (TNF- α) [11].

Progress in CRC has continued rapidly in recent years, and many studies have shown that the regulation of TAMs can effectively reduce the occurrence of tumors. For example, inhibition of M2 macrophage polarization prevents colitis-associated tumorigenesis [12, 13]. These results have been verified in the carcinogen-induced azoxymethane/dextran sulfate sodium (AOM/DSS) mouse model. The AOM/DSS model of colon cancer is widely used to investigate the roles of dietary factors in tumor development [14, 15].

Meanwhile, a more accurate in vitro CRC model that can physiologically replicate the key features of the human tissue has attracted increasing attention. Recent three-dimensional models not only better replicate mechanical stresses of natural tissue but also are more representative of the pathophysiological condition than classic monolayer cultures [16, 17]. Organoids are regarded as powerful technology bridges between conventional two-dimensional in vitro and in vivo models and have great potential for preclinical applications, especially in cancer research. Organoids have been successfully established for multiple types of cancer, such as stomach [18, 19], colorectal [18, 20, 21], liver [22, 23], pancreatic [24–26], prostate [27, 28], breast [29, 30], bladder [31, 32], and ovarian cancer [33].

Ginkgo biloba, a promising herb, has been used as a traditional herbal medicine for the past several thousand years [34, 35]. *G. biloba* leaf extracts have shown several

biological activities and are suggested to possess antitumor [36], antiaging [37], hepatoprotective [38], cardioprotective [39], and neuroprotective properties [40, 41]. In our previous study [42], we showed that bilobalide, a leaf extract of *G. biloba*, alleviated DSS-induced experimental colitis by inhibiting macrophage polarization of M1 through the nuclear factor kappa B signaling pathway. Similarly, many studies have suggested that the anti-inflammatory effects of *G. biloba* leaf extracts can contribute to the improvement of cardiovascular and neurological diseases [43–46]. Together, these findings demonstrate the anti-inflammatory activity of *G. biloba* leaf extract. CRC is closely associated with inflammation, but no studies have reported on the treatment of CRC with bilobalide.

Here, we investigate the suppressive effects of bilobalide on M2 macrophages and further examine the ability of bilobalide to prevent CRC in organoids and models of AOM/DSS mice. The findings of the present study improve our understanding of the anticancer effects of bilobalide and may contribute to the development of therapeutics against CRC.

2. Results

2.1. Bilobalide Inhibits M2 Macrophage Polarization In Vitro. As shown in Figure 1, bilobalide significantly reduced IL-10 and Arg-1 expression in a dose-dependent manner. Similar to the RT-qPCR analysis (Figure 1(b)), bilobalide significantly inhibited M2 markers (CD206, CCL22, fibronectin 1, and Arg-1) in a dose-dependent manner. We then determined the effect of bilobalide on the protein expression of representative M2 markers by Western blotting and immunofluorescence and found that bilobalide significantly decreased the levels of M2 markers (Figures 1(c) and 2(a)).

TAM can be classified into two phenotypes: M1 and M2. Briefly, M1 macrophages kill tumor cells, whereas M2 macrophages promote tumor growth. TAMs are usually present in the M2 polarization state in the tumor microenvironment. We hypothesized that the suppression of M2 macrophages by bilobalide may inhibit the progression of CRC.

To determine whether bilobalide inhibits M2 macrophage polarization and identify potential pathways that could be regulated, we used the M2 macrophage model of macrophages to identify. As shown in Figure 2(b), STAT3, JNK, and ERK phosphorylation in THP-1 cells was elevated after PMA/IL-4 treatment. We found that bilobalide inhibited STAT3, JNK, and ERK activation in a concentration-dependent manner.

2.2. Bilobalide Suppresses CRC Organoid Growth In Vitro. As shown in Figures 3(a) and 3(b), we cocultured CRC organoids and macrophages and monitored the formation and growth of CRC organoids for 10 days. The M2 group was the coculture group, and in addition to M2 macrophages, 10 μ M bilobalide was added to the Bil + M2 group. Specific markers (SRY-box transcription factor 9 and Ki67) of the CRC organoids were highly expressed (Figure S1-A),

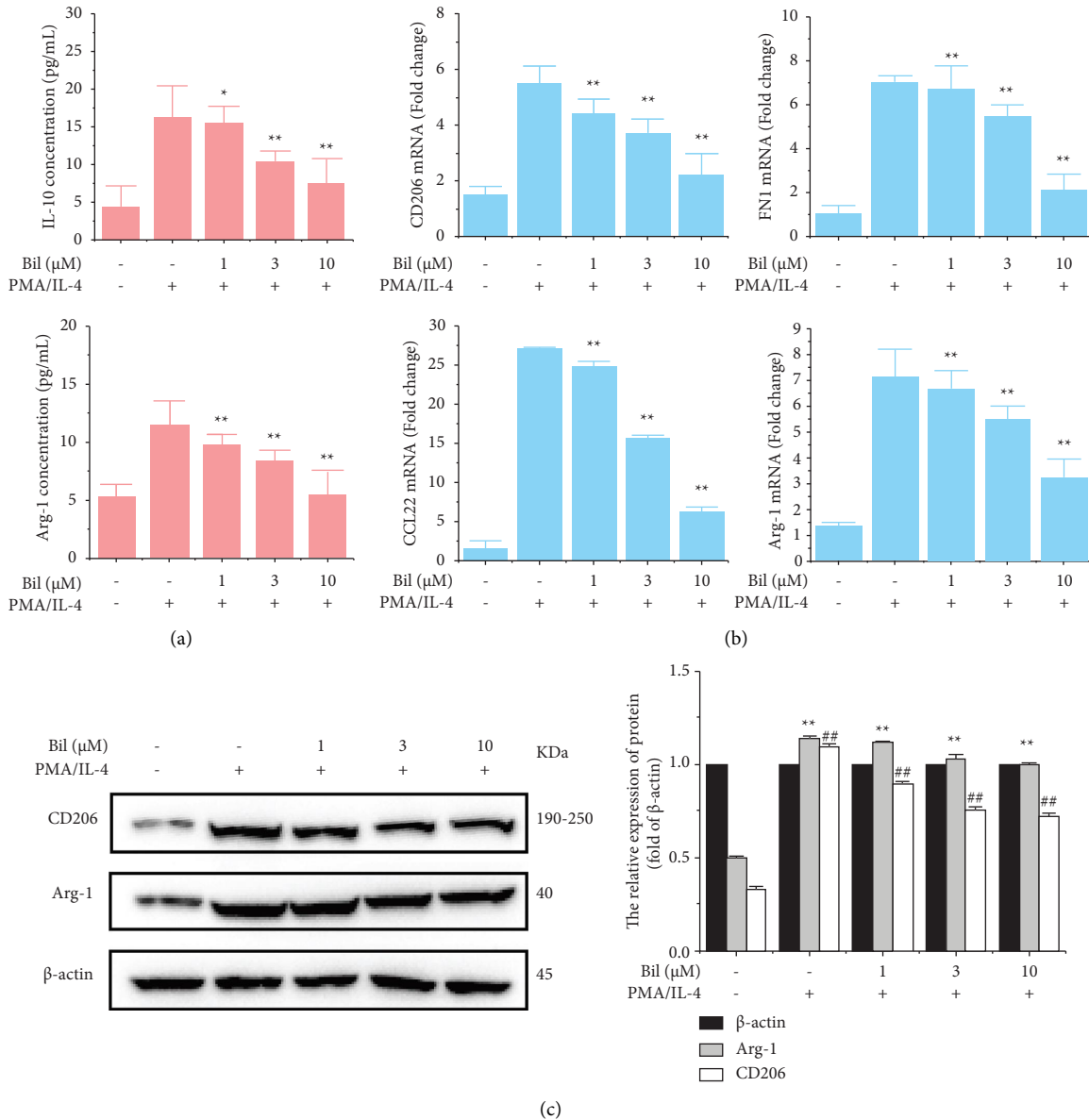


FIGURE 1: Bilobalide inhibits M2 macrophage polarization. (a) Concentration of IL-10 and Arg-1, * $P < 0.05$ and ** $P < 0.01$ compared with the Bil-PMA/IL-4+ group. (b) The mRNA levels of markers of M2 polarization of macrophages (CD206, CCL22, fibronectin 1, and Arg-1), ** $P < 0.01$ compared with the Bil-PMA/IL-4+ group. (c) Protein expression of CD206, Arg-1, and β -actin, ** $P < 0.01$ and ## $P < 0.01$ compared with β -actin.

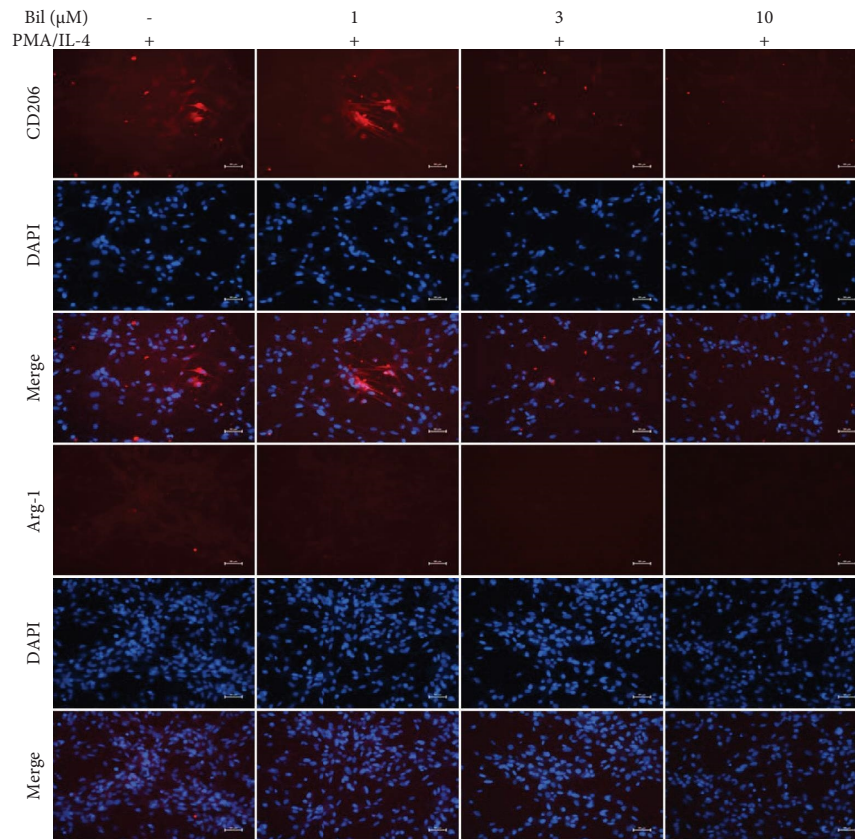
demonstrating the successful establishment of CRC organoids. Analysis of the CRC organoid images on days 1, 3, 6, and 10 revealed distinct differences in their morphology. The images showed that bilobalide treatment dramatically inhibited the growth of CRC organoids compared to the M2 and blank groups. The size of CRC organoids was smaller in the group treated with bilobalide than in the M2 or blank groups.

As shown in Figure 3(c), the cell viability of the M2 group was higher than that of the blank and Bil + M2 groups. The viability of the CRC organoids was significantly reduced in the bilobalide-treated group compared to the blank or M2 groups. As shown in Figure 3(d), the diameter of CRC organoids in the blank and M2 groups increased remarkably

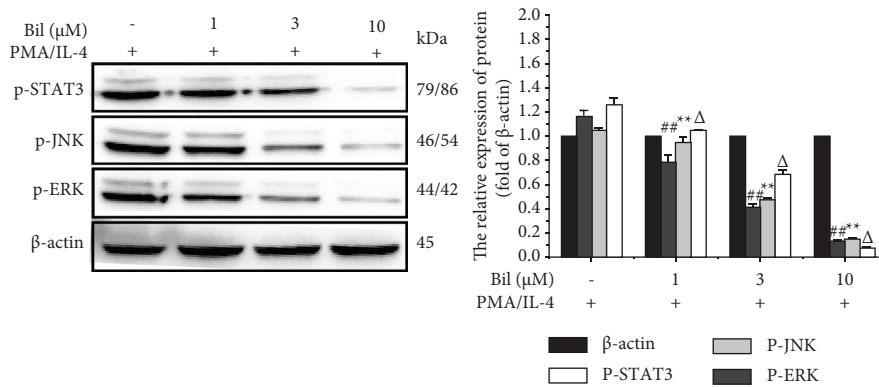
with time. However, there was no significant change in the organoid diameter of the Bil + M2 group. The change in organoid diameters may be explained by cellular reorganization. Importantly, bilobalide alone had little effect on the viability of CRC organoids (Figure S1-B).

These data indicated that bilobalide had an inhibitory effect on human patient-derived CRC organoids. It is plausible that the inhibitory effect of bilobalide may have been due to the suppression of M2 macrophage polarization.

2.3. Bilobalide Inhibits Inflammation and Promotes Apoptosis to Restrict CRC Organoid Growth In Vitro. Based on the aforementioned results, an ELISA was performed to



(a)



(b)

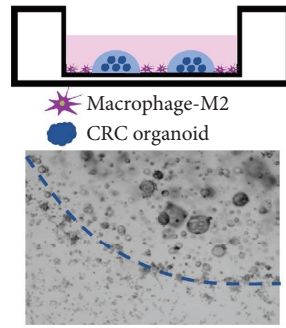
FIGURE 2: Bilobalide inhibits M2 macrophage polarization and detection of some pathways. (a) Immunofluorescence of CD206 and Arg-1. (b) Relative expression of p-STAT3, p-JNK, p-ERK, and β-actin, ** $P < 0.01$, ## $P < 0.01$, and $\Delta P < 0.01$ compared with β-actin.

measure cytokine levels in the culture supernatant. As shown in Figure 4(a), there was an increase in IL-10 concentration in the coculture system (M2 group). However, bilobalide treatment (Bil + M2 group) caused a decrease and increase in IL-10 and TNF-α concentration, respectively.

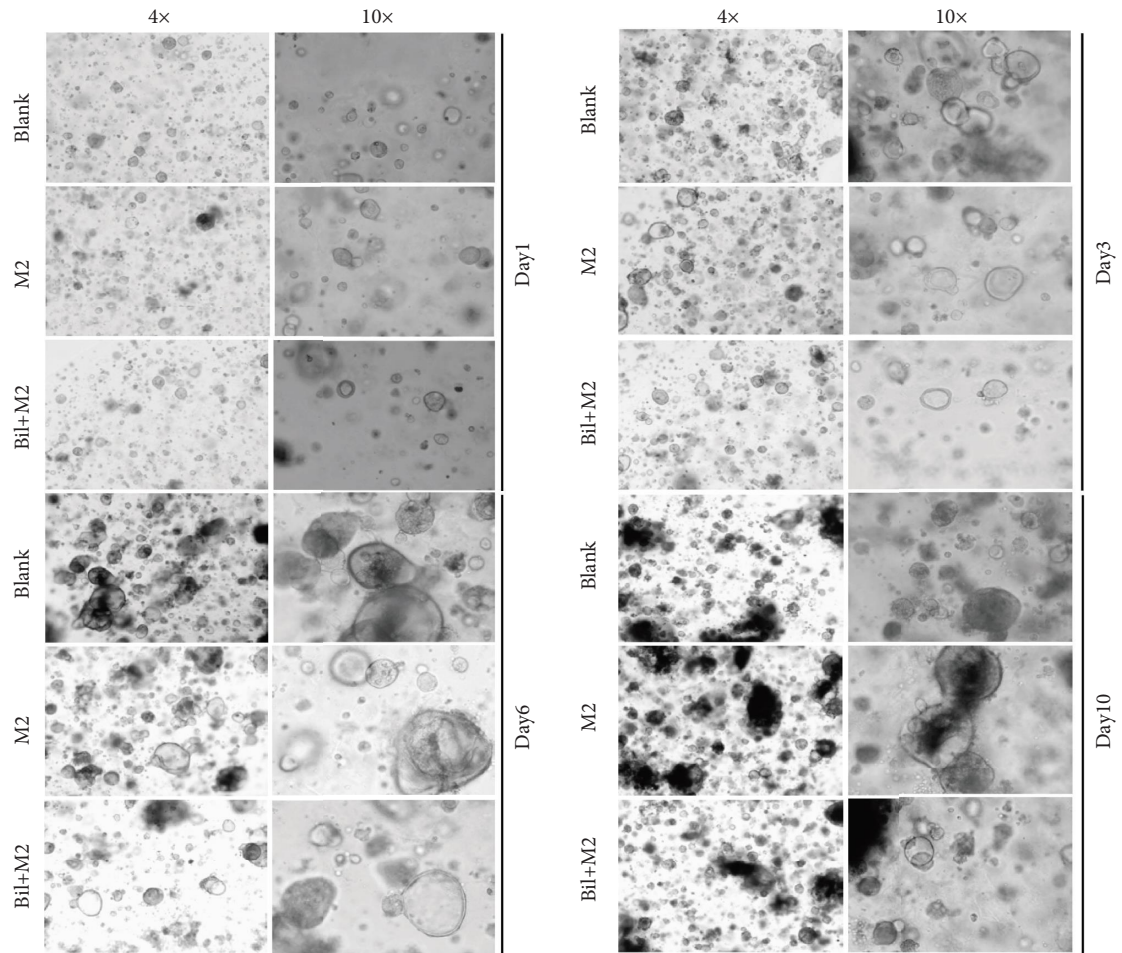
Meanwhile, Western blot analysis of the expression levels of cell apoptosis-associated proteins (Figure 4(b)) showed that the apoptotic markers B-cell lymphoma 2-associated X protein (Bax) and caspase 3 were markedly

upregulated in the M2 and Bil + M2 groups, whereas B-cell lymphoma 2 (Bcl-2) protein expression levels were suppressed. TUNEL staining (Figure 4(c)) showed that the proportion of CY3-positive cells (undergoing apoptosis) in bilobalide-treated organoids was significantly higher than that in the other groups.

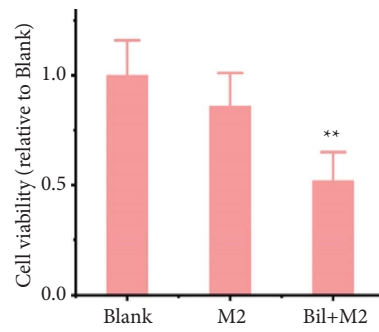
These data suggest that bilobalide inhibited the viability of CRC organoids and induced apoptosis, which may be attributed to the transformation of M2 macrophages to the M1 phenotype.



(a)



(b)



(c)

FIGURE 3: Continued.

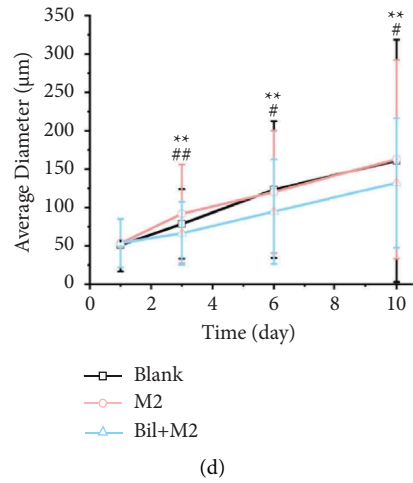


FIGURE 3: CRC organoids and M2 macrophage coculture systems. (a) Schematic representation of the coculture system. (b) Morphology of the CRC organoids on days 1, 3, 6, and 10. (c) Cell viability of the CRC organoids, $**P < 0.01$ compared with the M2 group. (d) Diameter of the CRC organoids for the different groups, $**P < 0.01$, the Bil + M2 group compared with the blank group; $##P < 0.01$ and $#P < 0.05$, the M2 group compared with the blank group.

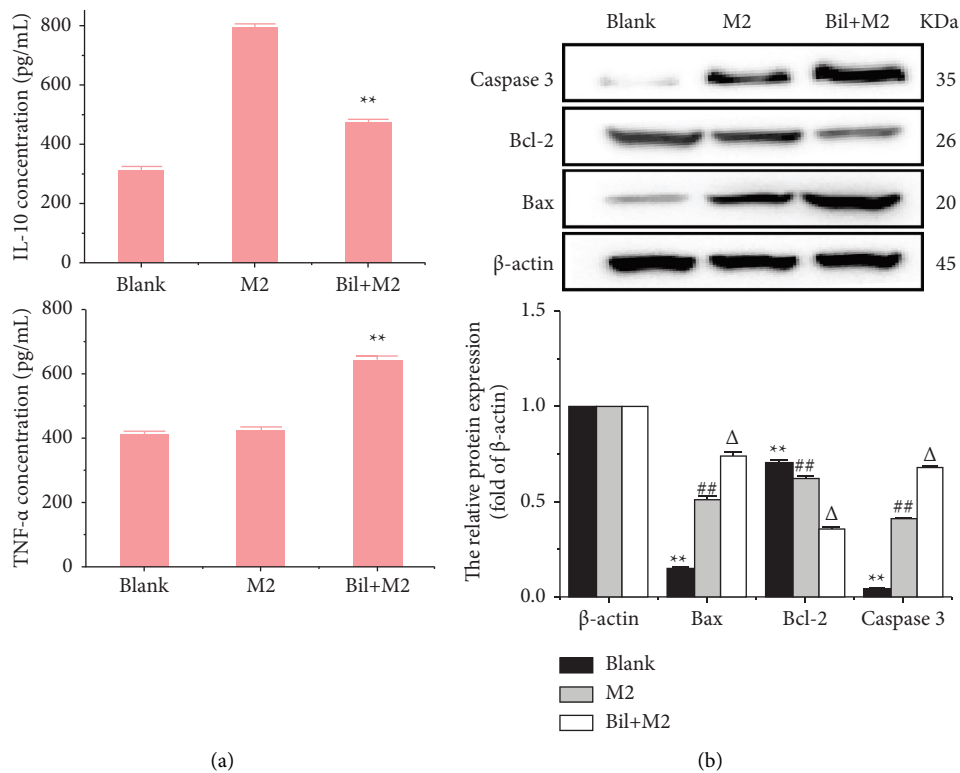


FIGURE 4: Continued.

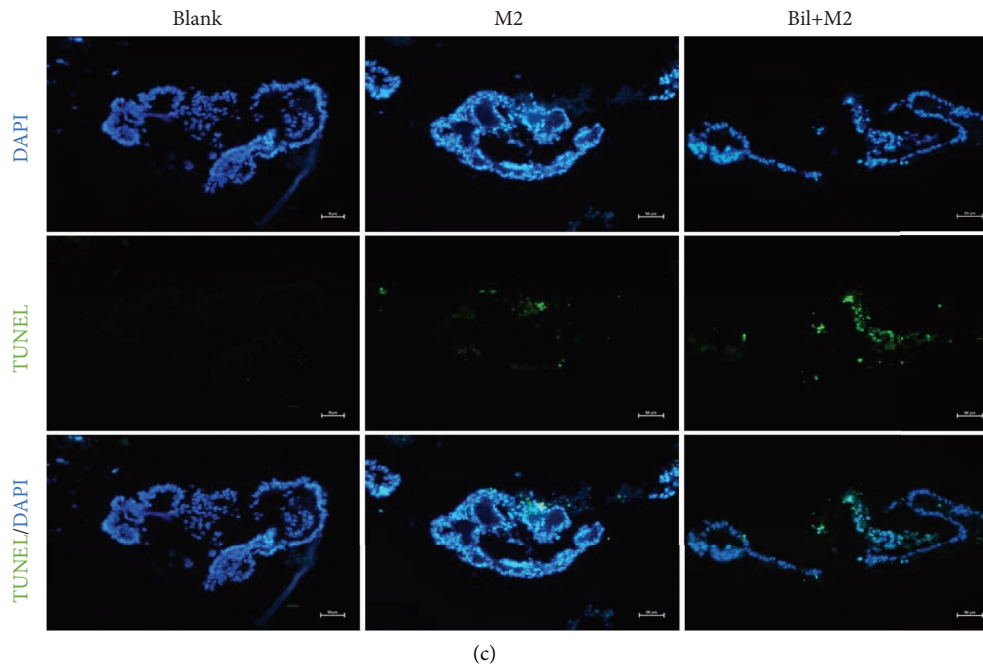


FIGURE 4: Bilobalide enhanced the apoptosis of the CRC organoids by inhibiting the polarization of M2 macrophages. (a) The concentration of IL-10 and TNF- α in the supernatants, ** $P < 0.01$ compared with the M2 group. (b) Relative expression of apoptosis-associated proteins, ** $P < 0.01$, the Bil + M2 group compared with the blank group, ** $P < 0.01$, ## $P < 0.01$, and $\Delta P < 0.01$ compared with β -actin. (c) TUNEL staining.

2.4. Bilobalide Prevents Intestinal Tumorigenesis in Mice.

To investigate the ability of bilobalide to prevent CRC formation, we established intestinal tumorigenesis in AOM/DSS mouse models (Figure 5(a)) and then monitored body weight, survival rate, and tumor incidence in these animals. As shown in Figure 5(b), there was a significant decrease in the body weight of mice from the AOM/DSS-treated group compared to that from the control group (drinking water). In addition, bloody stools were observed in the AOM/DSS group. However, compared to the AOM/DSS-treated groups, the body weights of mice from the treatment groups improved significantly after bilobalide (2.5 or 5 mg/kg, i.g.) treatment. Furthermore, mice treated with 5 mg/kg bilobalide showed greater weight recovery than mice that received a 2.5 mg/kg dose. According to Figure 5(c), bilobalide treatment remarkably improved survival in mice. Specifically, the survival rates were 80% and 90% for mice treated with 2.5 mg/kg and 5 mg/kg bilobalide, respectively.

The incidence (percentage of mice with colon adenomas) of colorectal tumors in AOM/DSS-treated mice was of 100% (Figure 5(f)), and the tumor size was 3.34 ± 0.30 mm (Figure 5(e)). Bilobalide treatment significantly decreased the colon adenoma incidence (25% for 2.5 mg/kg and 66.67% for 5 mg/kg) and tumor size (9.53% for 2.5 mg/kg and 44.24% for 5 mg/kg) (Figure 5(e)). In particular, DSS administration resulted in a notable decrease in colon length, while bilobalide treatment significantly improved colon contractibility (Figure 5(g)). Bilobalide dose dependently decreased the colon weight/length ratio in mice with AOM/DSS-induced colitis.

Collectively, these results demonstrate that bilobalide could protect mice against AOM/DSS-induced colitis-associated tumorigenesis, which may be attributed to the anti-inflammatory and antitumor properties of bilobalide.

2.5. Effect of Bilobalide on Histological Alteration and Cytokine Levels.

Next, we evaluated histological alterations in the colorectum to confirm the anticarcinogenic effect of bilobalide. As shown in Figure 5(h), it shows the normal structure of the colon, without infiltration of inflammatory cells in the control group. In the AOM/DSS group, tumor tissue is inside the colonic mucosa, with a small amount of necrotic tissue in the middle of the tumor. Furthermore, the colon tissue showed dense glands, a sieve-shaped pore structure, obvious atypical hyperplasia of glandular epithelial cells, obvious nuclear enlargement and pathological mitosis, and infiltration of inflammatory cells into the stroma, according to the signs of adenoma (tubular adenoma). However, the 5 mg/kg dose group showed tumor tissue in colonic mucosa, but with less atypia, and the structural change of colon was not obvious in most cases, and the glands were arranged neatly in most cases.

As indicated in Figure 6(a), ELISA was performed to evaluate the serum levels of proinflammatory cytokines. We observed that the concentration of proinflammatory cytokines (TNF- α , IL-1 β , and IL-6) in AOM/DSS mice was significantly higher than that in normal mice. Changes in cytokine levels were substantially reduced in mice in the treatment group compared to those in the AOM/DSS control

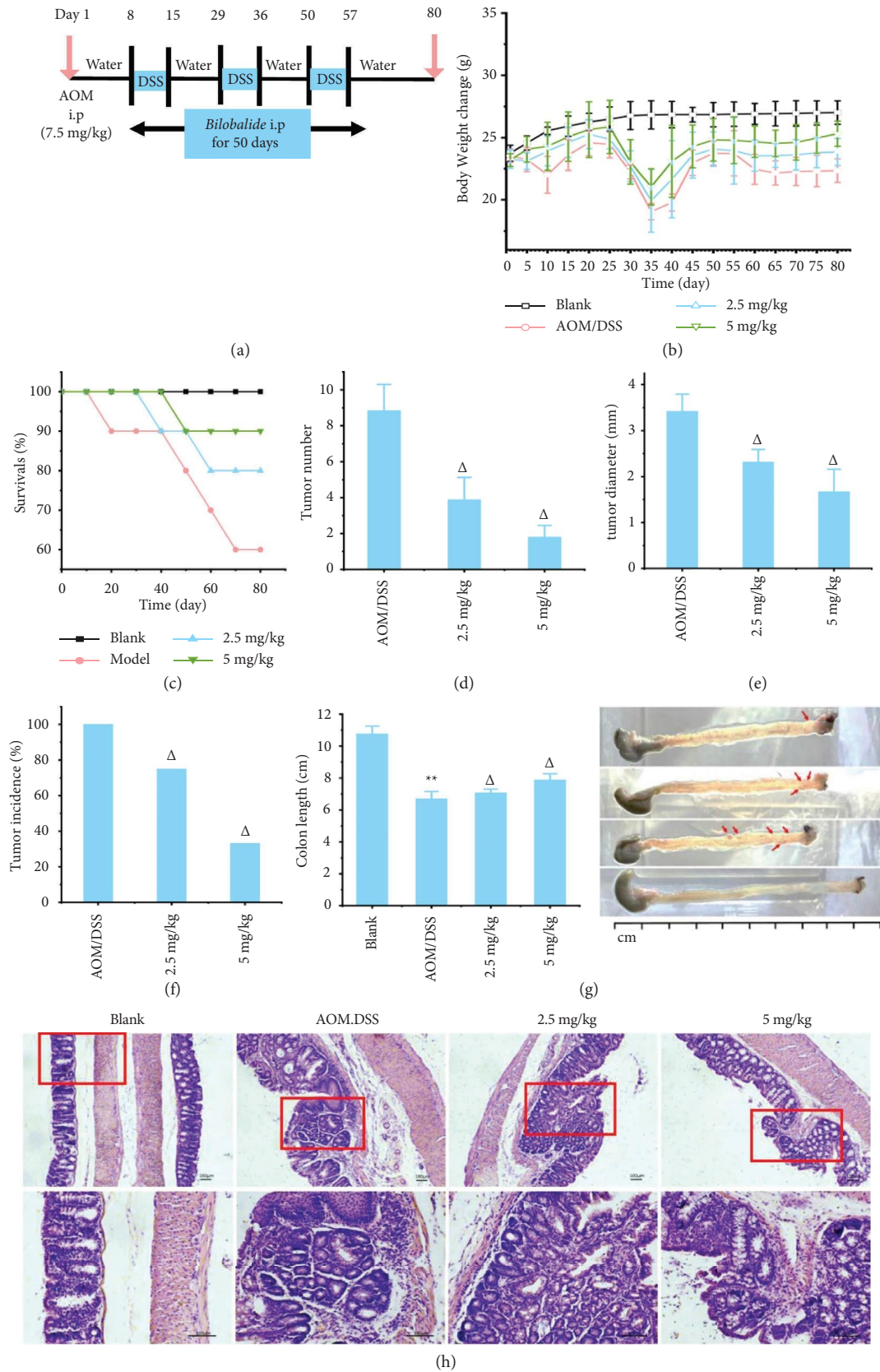


FIGURE 5: Bilobalide prevented intestinal tumorigenesis in mice. (a) Schematic representation for the establishment of the AOM/DSS mice model. (b) Changes in the body weights of mice from the control, model, 2.5 mg/kg bilobalide, and 5 mg/kg bilobalide groups. (c) Survival rates of mice from the control, model, 2.5 mg/kg bilobalide, and 5 mg/kg bilobalide groups. (d-f) Change in the tumor number, tumor size and incidence. (g) Change in the length and morphology of the colon. (e) Change in the length and morphology of the colon. (h) Effect of bilobalide on histological alteration. ($\Delta P < 0.01$ compared with AOM/DSS group, $**P < 0.01$ compared with blank group).

group when bilobalide (2.5 and 5 mg/kg) was administered. In particular, there was a decrease in the concentration of IL-10 after the administration of bilobalide. Meanwhile, the activity of MDA, LPO, and GSH was also measured as shown in Figure 6(b). Compared to the control and AOM/DSS groups, AOM/DSS alone caused a significant increase in MDA and LPO while decreasing the GSH content. Co-administration of bilobalide (2.5 and 5 mg/kg) with AOM/DSS reduced the level of MDA and LPO while increasing the level of GSH. Overall, these findings showed that bilobalide could effectively relieve symptoms in the AOM/DSS mouse model, which may be due to the inhibition of M2 polarization and suppression of inflammation and oxidative stress.

2.6. Macrophage Polarization Is Involved in the Preventive Effects of Bilobalide. To further verify our findings on the ability of bilobalide to prevent colorectal carcinoma, we performed immunohistochemical staining to examine the expression of cancer genes and macrophage subtype markers in colon tumors. Protein levels of Ki67, PCNA, c-Myc, and CD206 in colon tissues were lower in mice in the bilobalide group than in mice in the AOM/DSS-induced colitis group (Figure 6(c)).

Thus, the anticancer effect of bilobalide is associated with the regulation of macrophage polarization in the intestinal microenvironment, and the inhibition of M2 polarization is critical for the prevention of CRC.

3. Discussion

Tumor environments have been shown to affect cancer cell progression. TAMs can be classified into two phenotypes based on their polarization: tumor-suppressive M1 and tumor-promoting M2 macrophages. Generally, macrophage polarization in the M2 phenotype is a fundamental event closely associated with tumor prognosis. Some studies indicate that the longer the course of the disease, the higher the risk of tumorigenesis. Additionally, chronic inflammation has been shown to promote the development of cancers like CRC [47–50]. Similarly, the M2 phenotype is an important risk factor for CRC development. The present study suggests that suppression of M2 polarization is a promising alternative to prevent CRC in AOM/DSS C57BL/6 models, which are commonly used to investigate the roles of some factors in vivo [11]. Increasing evidence indicates that extracts from traditional herbal medicines, such as isoliquiritigenin (extracted from licorice) [13], the active fractions of *Garcinia* [12], triptolide [51], and *G. biloba* extract [52] can participate in the CRC process by regulating TAMs. For example, isoliquiritigenin effectively inhibits colitis-associated tumorigenesis by blocking the polarization of M2 macrophages by negatively regulating PGE2 and IL-6 signaling [13]. YTE-17, the active fractions of *Garcinia*, significantly decreased colitis-associated tumorigenesis by regulating M2 macrophage polarization [12]. Our results showed that Bil also inhibits M2 macrophage polarization and suppresses the progression of CRC. Interestingly, our study tested the effects of Bil on colon cancer development by using two

models: CRC organoids/THP-1 coculture model and the AOM/DSS-induced CRC model. With the advantage of three-dimensional culturing, organoids have been established and regarded as miniatures of in vivo tissues and organs [53]. Organoids can serve as experimental and preclinical models due to their ability to recapitulate some of the key structural and functional features of organs ex vivo.

In our study, THP-1 cells were polarized into the M2 phenotype using 100 µg/mL PMA and 20 µg/mL IL-4. Polarized M2 macrophages were treated with bilobalide. The results of ELISA, qPCR, Western blotting, and immunofluorescence showed that the markers of macrophages M2 (Arg-1, IL-10, and CD206) were significantly suppressed. Meanwhile, the expression of p-ERK, p-JNK, and p-STAT3 decreased in a dose-dependent manner after the administration of 2.5 mg/kg and 5.0 mg/kg, indicating that bilobalide inhibited STAT3, JNK, and ERK signaling pathways. STAT3, ERK, and JNK play critical roles in the transcriptional regulation of genes that encode inflammatory mediators. Consequently, the phosphorylation of STAT3, JNK, and ERK in THP-1 cells was suppressed by bilobalide, indicating that bilobalide is involved in the regulation and attenuation of inflammation. Similarly to Hua Sui's work [13], the present study shows that Bil may block M2 macrophage polarization more significantly by downregulating JNK, STAT3, and ERK signaling.

Organoids serve as a bridge for in vitro and in vivo research. Therefore, CRC organoids were cultured to investigate the relationship between M2 polarization and CRC. After culturing of CRC organoids, M2 macrophages obtained after treating THP-1 cells with PMA/IL-4 were cocultured with CRC organoids (M2 group). We detected the average diameter of the organoids on days 1, 3, 6, and 10 and observed visible inhibition of organoid growth in the Bil + M2 group. Cell viability for the Bil + M2 group on day 10 was significantly decreased compared to that for the blank and M2 groups. On day 10, we observed a nonsignificant decrease in the cell viability of the M2 group compared to that of the blank group. The change in the M2 group was associated with the mutual promotion of the microenvironment obtained from M2 phenotype and tumors. Based on these results, we concluded that the viability of bilobalide-treated CRC organoids showed significant suppression. Regarding inflammatory cytokines, it was obvious that there was an increase in the levels of IL-10 in the coculture group. Bilobalide remarkably inhibited TAM expression by suppressing IL-10, which is considered the main M2 marker, and upregulating the main M1 markers, including TNF-α. Meanwhile, apoptosis levels were assessed by Western blotting and TUNEL staining in the three groups (blank, M2, and Bil + M2 groups). The proportion of fluorescein-positive cells was indicative of apoptosis. There was an increase in the ratio of TUNEL-positive cells in the Bil + M2 group compared to that in the blank and M2 groups. Furthermore, it was worth exploring the anticancer mechanism of bilobalide based on CRC organoids.

The results of the AOM/DSS mouse model confirmed the inhibitory effects of bilobalide on CRC. Treatment with bilobalide (especially with 5 mg/kg) could significantly prevent colon length shortening, prolong survival rate,

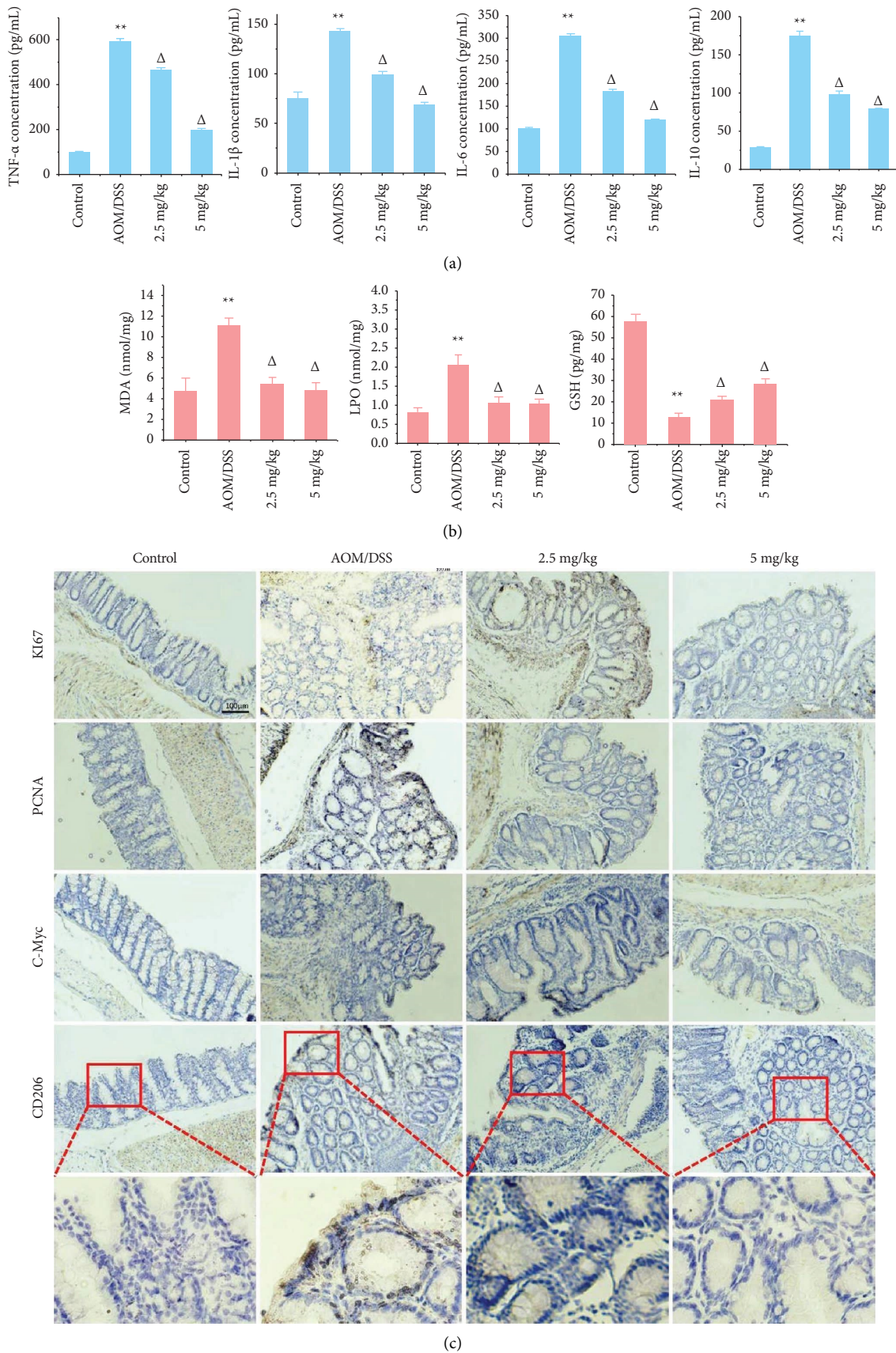


FIGURE 6: Bilobalide improved AOM/DSS mice model as detected ELISA and immunohistochemical staining. (a) Changes in the concentration of TNF- α , IL-1 β , IL-6, and IL-10. (b) Changes in the activity of MDA, LPO, and GSH. (c) Changes in the expression of Ki67, PCNA, c-Myc, and CD206 in the IHC of colonic tissues. $\Delta P < 0.01$ compared with the AOM/DSS group; $**P < 0.01$ compared with the control group.

improve the decrease in disease activity index (DAI) death rate, and prevent the loss of body weight. The coexistence of oxidative stress and inflammation accelerates neoplastic transformation [54]. In this study, the decreased MDA and LPO level with a concomitant upregulation in GSH level also indicated the successful suppression of oxidative stress in the colon of AOM/DSS mice treated to bilobalide. Treatment with bilobalide caused a downregulation in the levels of proinflammatory cytokines (TNF- α , IL-1 β , and IL-6). However, compared to the normal group, there was an increase in the levels of IL-10 in the AOM/DSS group and decreased after treatment with bilobalide, which may be due to the inhibition of M2 polarization. TNF- α and IL-6 are responsible for inducing the M1 phenotype, whereas IL-4 and IL-10 are M2-polarizing cytokines. Furthermore, the immunohistochemical staining results revealed that compared to the AOM/DSS group, the expression of PCNA, Ki67, c-Myc, and CD206 was downregulated in the bilobalide-treated groups. Collectively, these findings indicated that bilobalide treatment could suppress M2 polarization and promote the transformation of M1 macrophages, which could alleviate inflammation and oxidative stress and prevent CRC.

In summary, bilobalide could effectively hamper the progression of CRC. The ability to restrain M2 macrophage polarization and inhibition of inflammation and oxidative stress suggests that bilobalide is a promising preventive or protective agent for attenuating CRC.

4. Materials and Methods

4.1. THP-1 Cell Culture and Polarization. The bilobalide was purchased from MedChemExpress Inc. The human monocytic THP-1 cell line was purchased from American Type Culture Collection (Rockville, MD) and cultured in Roswell Park Memorial Institute developed 1640 medium (Gibco, Grand Island, NY) containing 10% fetal bovine serum (Gibco, Grand Island, NY) and 1% penicillin-streptomycin at 37°C and 5% CO₂ for 5 days. The macrophages were washed twice with phosphate-buffered saline (PBS), prior to culturing the cells in fresh Roswell Park Memorial Institute developed 1640 medium supplemented with 10% fetal bovine serum, 100 ng/mL PMA (M0), and 20 ng/mL IL-4 (M2 polarization) for 24 h.

4.2. Inflammatory Biomarkers and Biochemical Assays. The enzyme-linked immunosorbent assay (ELISA) kits obtained from Yubo Co. Ltd. (Shanghai, China) were used to quantify the levels of TNF- α , IL-1 β , IL-6, IL-10, IL-4, and Arg-1 in the supernatant and animal sera.

The total protein content was determined by bicinchoinic acid assay (BCA assay) (SolarBio, Beijing, China). Lipid peroxide (LPO) levels, malondialdehyde (MDA) activity, and reduced glutathione (GSH) activity were analyzed using commercially available assay kits from Yubo Co. Ltd. (Shanghai, China). The specific experimental procedures were performed according to the manufacturer's instructions.

4.3. Immunofluorescence. Cells or sections were immobilized using 4% paraformaldehyde (PFA) (Sigma-Aldrich, USA), permeabilized with 0.5% Triton X-100 (Sigma-Aldrich, USA) for 20 min, and thereafter sealed with 5% bovine serum albumin (Gibco, Grand Island, NY) for 30 min. The cells were incubated overnight with anti-mouse Arg-1 (1:200-1:1000 dilution, Proteintech, catalog number: 66129-1), anti-mouse CD206 (1:200-1:1000 dilution, Proteintech, catalog number: 60143-1), anti-rabbit iNOS (1:200-1:1000 dilution, Proteintech, catalog number: 22226-1), and anti-rabbit Ki67 (1:200-1:1000 dilution, Proteintech, catalog number: 27309-1) antibodies for immunostaining. Next, the cells were treated with Alexa Fluor 488/Cy3-conjugated anti-mouse/rabbit immunoglobulin G (Life Technology, CA) for 2 h at 37°C. Thereafter, 4',6-diamidino-2-phenylindole was applied to counterstain the coverslips and the samples imaged under fluorescence microscopy (Nikon, Japan).

4.4. Quantitative Real-Time Polymerase Chain Reaction. Total RNA was isolated from cells or tissues using the TRIzol reagent (Invitrogen, Carlsbad, CA, USA). Total RNA was reverse transcribed into complementary DNA and subjected to quantitative real-time polymerase chain reaction (RT-qPCR) analysis using the ABI 7500 detection system (Applied Biosystems, CA, USA) using ChamQ Universal SYBR qPCR Master Mix (Vazyme, China). The Bio-Rad CFX Manager software was then used to obtain the threshold cycle numbers. The amplification program was as follows: 2 min at 95°C for 1 cycle, followed by 10 s at 95°C for 40 cycles, 30 s at 60°C, and then 30 s at 72°C. Next, β -actin was used as an endogenous control to normalize the differences in total RNA. The comparative CT method, also referred to as the $2^{-\Delta\Delta CT}$ method, where fold change = $2^{-\Delta\Delta CT} = [(CT \text{ gene of interest} - CT \text{ gene of actin control}) \text{ sample A} - (CT \text{ gene of interest} - CT \text{ gene of actin control}) \text{ sample B}]$, was used to calculate the relative gene expression. Primer sequences used in this study are listed in Table 1.

4.5. CRC Organoid Culture. Fresh tumor tissues from colorectal cancer patients were washed with cold Hank's balanced salt solution (Sigma-Aldrich, USA). After removing the muscle tissue, the epithelial tumor tissues were cut into small pieces and vigorously suspended in wash solution (DMEM/F-12 medium + 1 \times HEPES + 1 \times GlutaMAX + 1% penicillin-streptomycin). The tissue suspension was then centrifuged at 140 rpm for 3 min to enrich the tumor fraction at the bottom of the tube. The fraction was incubated at 37°C on a shaker at medium speed (140 rpm, 30 min) following the addition of 2-3 mL of the digestion solution (DMEM/F-12 medium + 5 mg/mL collagenase + 10 μ g/mL DNase I). The supernatant was aspirated, and the cell pellets were retained. Pellets embedded in 5 mL Matrigel (Corning, catalog number: 354234) were seeded into 6-well plates and cultured in conditioned medium after solidification of the Matrigel. The Matrigel was composed of 50% WNT3A conditioned medium, 10% R-spondin conditioned medium, 38% advanced DMEM/F-12 (Gibco),

TABLE 1: Primer sequences used for real-time RT-PCR.

Gene	Primer sequences	
	Forward	Reverse
CD206	GCAAAGTGGATTACGTGTCTTG	CTGTTATGTCGCTGGCAAATG
CCL22	GAGCATGGATCGCTACAG	CAGACGGTAACGGACGTAATC
FN1	ACTGTACATGCTTCGGTCAG	AGTCTCTGAATCCTGGCATTG
Arg-1	CATATCTGCCAAAGACATCGTG	GACATCAAAGCTCAGGTGAATC
GAPDH	CAACGGATTGGTCGTATTGG	TGACGGTGCCATGGAATT

1 × B27, 1.25 mmol/L N-acetyl cysteine, 10 mmol/L nicotinamide, 50 ng/mL EGF (Sigma), 500 nmol/L A83-01, 100 ng/mL noggin, and 10 mmol/L Y-27632.

4.6. Cell Viability Assay. Cell viability assay for CRC organoids was carried out using the CellTiter-Lumi™ Plus Luminescent Cell Viability Assay Kit (Beyotime, CN). Briefly, 4×10^3 cells from each CRC organoid were embedded in 100 μ L Matrigel in a 24-well culture plate containing mentioned culture media for 5 days. M2-polarized THP-1 cells were seeded into CRC organoids for coculturing, and the cocultured cells were treated with bilobalide (10 μ M) for 10 days. The viability of organoids was measured using CellTiter-Lumi™ Plus Luminescent Cell Viability Assay Kit.

The immunofluorescence and terminal deoxynucleotidyl transferase biotin-dUTP nick end labeling (TUNEL) staining were operated according to the manufacturer's instructions.

4.7. Induction of AOM-Initiated and DSS-Promoted Colon Carcinogenesis and Treatment. 40 C57BL/6 mice (male, 6–8 weeks old, 18–22 g) were obtained from the Laboratory Animal Center of Jiangsu University (Zhenjiang, China). All animals were grouped randomly at a specific-pathogen-free facility, where the temperature was controlled at $22 \pm 2^\circ\text{C}$, and the lighting conditions were constantly circulated (12 h of light and 12 h of darkness). The animal experiments were approved by the Animal Experimental Ethical Committee of Jiangsu University and were carried out at the Laboratory Animal Research Center of Jiangsu University (No. UJS-IACUC-2022081503). Every effort was made to reduce the number of animals used and minimize their suffering. The 40 mice were randomly divided into four groups ($n = 10$, per group) such as control, AOM/DSS, bilobalide (2.5 mg/kg), and bilobalide (5.0 mg/kg) groups. The selection of bilobalide dose was based on our previous study [42]. The procedures used for treatment schedule of the CRC model by AOM and DSS are shown in Figure 5(a) and Table 2. Briefly, mice were injected with AOM (7.5 mg/kg [55], intraperitoneally) on day 1. After one week, the mice were administered 2.5% DSS in their drinking water for one week, which was followed by two weeks of tap water for recovery. This cycle was repeated thrice. Bilobalide (2.5 or 5 mg/kg, the dissolution method was provided in the instructions provided by MCE) was administered orally for 12 weeks during the period of DSS administration.

4.8. Histology, Immunohistochemistry, and Immunofluorescence. Blood collected from the retinal venous plexus was centrifuged (3700 rpm/min, 5 min) to harvest serum, which was stored at -80°C for future use. The mice were sacrificed by cervical dislocation. The whole intestine was removed immediately after the sacrifice and dissected longitudinally after washing with ice-cold PBS (Sigma-Aldrich, USA), as described previously [47]. The number, location, and size of visible tumors throughout the intestine were measured to calculate the incidence of adenomas. Tumor numbers were counted and grouped based on size as follows: <2 mm, 2–4 mm, and >4 mm. The tissue sections were fixed in 10% formalin (Sigma-Aldrich, USA) and thereafter embedded in paraffin. The sections were stained with hematoxylin and eosin (Sigma-Aldrich, USA) for pathological evaluation, which was performed by a pathologist who was blinded to the experimental groups. Histopathological analysis of the neoplastic lesions and degree of dysplasia were performed according to the standard criteria for the classification of colon adenomas.

Regarding the murine samples, immunohistochemistry was performed using anti-rabbit cellular Myc (c-Myc, Abcam, catalog number: ab32072), anti-mouse CD206 (Proteintech, catalog number: 60143-1), anti-mouse Ki67 (Proteintech, catalog number: 27309-1), anti-mouse proliferating cell nuclear antigen (PCNA, Abcam, catalog number: ab29), and the colorimetric TUNEL Apoptosis Assay Kit (Beyotime, CN). All stains used a horseradish peroxidase-conjugated antibody. Chromogenic detection was performed with the substrate 3-3'-diaminobenzidine and counterstaining with hematoxylin.

4.9. Western Blotting. Colonic tissues of the mice were lysed in RIPA lysis buffer. After centrifugation at 10,000 g for 20 min at 4°C , the supernatants were collected and protein concentrations were measured using a bicinchoninic acid assay kit (Thermo Fisher, MA, USA). Electrophoresed samples were separated by 10% sodium dodecyl sulfate polyacrylamide gel electrophoresis (SDS-PAGE) and transferred onto polyvinylidene difluoride membranes (Millipore, MA, USA) and blocked using 5% fat-free milk for 1 h at $18\text{--}25^\circ\text{C}$. After washing in PBST (1 × PBS, 0.1% Tween® 20 Detergent), the membranes were incubated with primary antibodies at 4°C overnight. The membranes were washed three times with PBST before the addition of horseradish peroxidase-labeled secondary antibodies. The signals were detected using chemiluminescent horseradish peroxidase substrate (Millipore) on a Bio-Rad imaging

TABLE 2: The treatment schedule of AOM/DSS mice.

Groups (n = 10)	Time (d)							
	1-7	8-14	15-28	29-35	36-49	50-56	57-79	80
Control					Water			
AOM/DSS	Normal saline	DSS (2.5%)	Water	DSS (2.5%)	Water	DSS (2.5%)	Water	
Bilobalide (2.5 mg/kg)	AOM (7.5 mg/kg, i.p.)	DSS (2.5%)	Water	DSS (2.5%)	Water	DSS (2.5%)	Water	Sacrifice
Bilobalide (5.0 mg/kg)		DSS (2.5%)	Water	Bilobalide (2.5 mg/kg, i.g.)	Water	DSS (2.5%)	Water	
				Bilobalide (5.0 mg/kg, i.g.)				

system (Bio-Rad ChemiDoc MP). Primary antibodies against the following proteins were used: Arg-1, CD206, inducible nitric oxide synthase (iNOS), phospho-extracellular signal-regulated kinase (p-ERK), phospho-c-Jun N-terminal kinases (p-JNK), phospho-signal transducer and activator of transcription 3 (p-STAT3), and beta-actin.

4.10. Statistical Analysis. All data are presented as mean \pm standard deviation. Differences between distinct groups were statistically evaluated using ANOVA and the least significant difference (LSD) test. Statistical significance was set at $P < 0.05$. All calculations were performed using SPSS version 19.0 (SPSS Inc., Chicago, IL, USA). All graphs were drawn using the Origin software (OriginLab Corp.).

Data Availability

The datasets generated for this study are available from the corresponding authors upon request.

Ethical Approval

The study was conducted in accordance with the Declaration of Helsinki and approved by the Ethics Committee of Jiangsu University (No. UJS-IACUC-2022081503). The human samples were approved by the IRB of Nanjing Lishui People's Hospital (No. 20211210-01).

Conflicts of Interest

The authors declare that they have no conflicts of interest.

Authors' Contributions

H.Z., S.F., D.W., and M.X. conceptualized the study. H.Z., S.F., N.C., and X.L. developed methodology and investigated the study. X.F., R.L., F.R., and X.L. wrote the original draft. H.Z., S.F., F.S., F.R., R.L., D.W., and M.X. reviewed and edited the article. All authors have read and agreed to the published version of the manuscript and have given approval to the final version of the manuscript.

Acknowledgments

The authors are thankful to the Animal Experimental Ethical Committee of Jiangsu University and the IRB of Nanjing Lishui People's Hospital for providing the necessary support to generate the manuscript. This study was supported by Medical Clinical Science and Technology Development Fund of Jiangsu University (JLY20180033), the National Natural Science Foundation of China (No. 82072754), the Jiangsu Provincial Key Research and Development Program (No. BE2018689), the Natural Science Foundation of Jiangsu Province (No. M2020011), and the Zhenjiang Key Research and Development Program (No. SH2018033).

Supplementary Materials

Supplementary Figure 1: S1-(A) Characterization of CRC organoids by immunofluorescence staining. S1-(B) Relative cell viability of the bilobalide (Bil) group. (*Supplementary Materials*)

References

- [1] X. Lin, Z. Yi, J. Diao et al., "ShaoYao decoction ameliorates colitis-associated colorectal cancer by downregulating proinflammatory cytokines and promoting epithelial-mesenchymal transition," *Journal of Translational Medicine*, vol. 12, no. 1, p. 105, 2014.
- [2] J. Ferlay, H. R. Shin, F. Bray, D. Forman, C. Mathers, and M. Parkin, "Estimates of worldwide burden of cancer in 2008: globocan 2008," *International Journal of Cancer*, vol. 127, no. 12, pp. 2893–2917, 2010.
- [3] S. Deng, A. Wang, X. Chen et al., "HBD inhibits the development of colitis-associated cancer in mice via the IL-6R/STAT3 signaling pathway," *International Journal of Molecular Sciences*, vol. 20, no. 5, p. 1069, 2019.
- [4] M. Krzystek-Korpacka, D. Diakowska, B. Kapturkiewicz, M. Bębenek, and A. Gamian, "Profiles of circulating inflammatory cytokines in colorectal cancer (CRC), high cancer risk conditions, and health are distinct. Possible implications for CRC screening and surveillance," *Cancer Letters*, vol. 337, no. 1, pp. 107–114, 2013.
- [5] C. R. Lichtenstern, R. K. Ngu, S. Shalpour, and M. Karin, "Immunotherapy, inflammation and colorectal cancer," *Cells*, vol. 9, no. 3, p. 618, 2020.
- [6] L. Liu, H. Gao, T. Wen, T. Gu, S. Zhang, and Z. Yuan, "Tanshinone IIA attenuates AOM/DSS-induced colorectal tumorigenesis in mice via inhibition of intestinal inflammation," *Pharmaceutical Biology*, vol. 59, no. 1, pp. 87–94, 2021.
- [7] N. R. West, S. McCuaig, F. Franchini, and F. Powrie, "Emerging cytokine networks in colorectal cancer," *Nature Reviews Immunology*, vol. 15, no. 10, pp. 615–629, 2015.
- [8] Y. R. Na, M. Stakenborg, S. H. Seok, and G. Matteoli, "Macrophages in intestinal inflammation and resolution: a potential therapeutic target in IBD," *Nature Reviews Gastroenterology & Hepatology*, vol. 16, no. 9, pp. 531–543, 2019.
- [9] Y. Le, H. Gao, R. Bleday, and Z. Zhu, "The homeobox protein VentX reverts immune suppression in the tumor microenvironment," *Nature Communications*, vol. 9, no. 1, p. 2175, 2018.
- [10] A. Salmaninejad, S. F. Valilou, A. Soltani et al., "Tumor-associated macrophages: role in cancer development and therapeutic implications," *Cellular Oncology*, vol. 42, no. 5, pp. 591–608, 2019.
- [11] M. A. F. Yahaya, M. A. M. Lila, S. Ismail, M. Zainol, and N. A. R. N. M. Afizan, "Tumour-associated macrophages (TAMs) in colon cancer and how to reeducate them," *Journal of Immunology Research*, vol. 2019, Article ID 2368249, 9 pages, 2019.
- [12] H. Sui, H. Tan, J. Fu et al., "The active fraction of *Garcinia yunnanensis* suppresses the progression of colorectal carcinoma by interfering with tumor-associated macrophage-associated M2 macrophage polarization in vivo and in vitro," *The FASEB Journal*, vol. 34, no. 6, pp. 7387–7403, 2020.

- [13] H. Zhao, X. Zhang, X. Chen et al., "Isoliquiritigenin, a flavonoid from licorice, blocks M2 macrophage polarization in colitis-associated tumorigenesis through downregulating PGE2 and IL-6," *Toxicology and Applied Pharmacology*, vol. 279, no. 3, pp. 311–321, 2014.
- [14] K. L. N. W. F. Dove, "APC and its modifiers in colon cancer," *Advances in Experimental Medicine & Biology*, vol. 656, pp. 85–106, 2009.
- [15] M. K. Takahashi and K. Wakabayashi, "Gene mutations and altered gene expression in azoxymethane-induced colon carcinogenesis in rodents," *Cancer Science*, vol. 95, no. 6, pp. 475–480, 2004.
- [16] M. A. Lancaster and J. A. Knoblich, "Organogenesis in a dish: modeling development and disease using organoid technologies," *Science*, vol. 345, no. 6194, Article ID 1247125, 2014.
- [17] J. H. Drost and H. Clevers, "Organoids in cancer research," *Nature Reviews Cancer*, vol. 18, no. 7, pp. 407–418, 2018.
- [18] G. Vlachogiannis, S. Hedayat, A. Vatsiou et al., "Patient-derived organoids model treatment response of metastatic gastrointestinal cancers," *Science*, vol. 359, no. 6378, pp. 920–926, 2018.
- [19] T. Seidlitz, S. R. Merker, A. Rothe et al., "Human gastric cancer modelling using organoids," *Gut*, vol. 68, no. 2, pp. 207–217, 2019.
- [20] M. Fujii, M. Shimokawa, S. Date et al., "A colorectal tumor organoid library demonstrates progressive loss of niche factor requirements during tumorigenesis," *Cell Stem Cell*, vol. 18, no. 6, pp. 827–838, 2016.
- [21] F. Weeber, M. van de Wetering, M. Hoogstraat et al., "Preserved genetic diversity in organoids cultured from biopsies of human colorectal cancer metastases," *Proceedings of the National Academy of Sciences of the U S A*, vol. 112, no. 43, pp. 13308–13311, 2015.
- [22] L. Broutier, G. Mastrogianni, M. M. Verstegen et al., "Human primary liver cancer-derived organoid cultures for disease modeling and drug screening," *Nature Medicine*, vol. 23, no. 12, pp. 1424–1435, 2017.
- [23] S. Nuciforo, I. Fofana, M. S. Matter et al., "Organoid models of human liver cancers derived from tumor needle biopsies," *Cell Reports*, vol. 24, no. 5, pp. 1363–1376, 2018.
- [24] L. Huang, A. Holtzinger, I. Jagan et al., "Ductal pancreatic cancer modeling and drug screening using human pluripotent stem cell- and patient-derived tumor organoids," *Nature Medicine*, vol. 21, no. 11, pp. 1364–1371, 2015.
- [25] T. Seino, S. Kawasaki, M. Shimokawa et al., "Human pancreatic tumor organoids reveal loss of stem cell niche factor dependence during disease progression," *Cell Stem Cell*, vol. 22, no. 3, pp. 454–467.e6, 2018.
- [26] H. Zhang and C. J. Kuo, "Personalizing pancreatic cancer organoids with hPSCs," *Nature Medicine*, vol. 21, no. 11, pp. 1249–1251, 2015.
- [27] D. Gao, I. Vela, A. Sboner et al., "Organoid cultures derived from patients with advanced prostate cancer," *Cell*, vol. 159, no. 1, pp. 176–187, 2014.
- [28] T. R. Shenoy, G. Boysen, M. Y. Wang et al., "CHD1 loss sensitizes prostate cancer to DNA damaging therapy by promoting error-prone double-strand break repair," *Annals of Oncology*, vol. 28, no. 7, pp. 1495–1507, 2017.
- [29] N. Sachs, J. de Ligt, O. Kopper et al., "A living biobank of breast cancer organoids captures disease heterogeneity," *Cell*, vol. 172, no. 1–2, pp. 373–386.e10, 2018.
- [30] R. E. Ranftl and F. Calvo, "Analysis of breast cancer cell invasion using an organotypic culture system," *Methods in Molecular Biology*, vol. 1612, pp. 199–212, 2017.
- [31] T. Yoshida, N. A. Sopko, M. Kates et al., "Three-dimensional organoid culture reveals involvement of Wnt/ β -catenin pathway in proliferation of bladder cancer cells," *Oncotarget*, vol. 9, no. 13, pp. 11060–11070, 2018.
- [32] S. H. Lee, W. Hu, J. T. Matulay et al., "Tumor evolution and drug response in patient-derived organoid models of bladder cancer," *Cell*, vol. 173, no. 2, pp. 515–528, 2018.
- [33] J. Jabs, F. M. Zickgraf, J. Park et al., "Screening drug effects in patient-derived cancer cells links organoid responses to genome alterations," *Molecular Systems Biology*, vol. 13, no. 11, p. 955, 2017.
- [34] D. G. Al-Adwani, W. M. Renno, and Y. Orabi, "Neurotherapeutic effects of Ginkgo biloba extract and its terpene trilactone, ginkgolide B, on sciatic crush injury model: a new evidence," *PLoS One*, vol. 14, no. 12, Article ID e0226626, 2019.
- [35] H. F. Zhang, L. B. Huang, Y. B. Zhong et al., "An overview of systematic reviews of ginkgo biloba extracts for mild cognitive impairment and dementia," *Frontiers in Aging Neuroscience*, vol. 8, p. 276, 2016.
- [36] Y. Zhang, A. Y. Chen, M. Li, C. Chen, and Q. Yao, "Ginkgo biloba extract kaempferol inhibits cell proliferation and induces apoptosis in pancreatic cancer cells," *Journal of Surgical Research*, vol. 148, no. 1, pp. 17–23, 2008.
- [37] B. J. Diamond, S. C. Shiflett, N. Feiwei et al., "Ginkgo biloba extract: mechanisms and clinical indications," *Archives of Physical Medicine and Rehabilitation*, vol. 81, no. 5, pp. 668–678, 2000.
- [38] S. R. Naik and V. S. Panda, "Antioxidant and hepatoprotective effects of Ginkgo biloba phytoosomes in carbon tetrachloride-induced liver injury in rodents," *Liver International*, vol. 27, no. 3, pp. 393–399, 2007.
- [39] T. Tunali-Akbay, G. Sener, H. Salvarli, O. Sehirli, and A. Yarat, "Protective effects of Ginkgo biloba extract against mercury(II)-induced cardiovascular oxidative damage in rats," *Phytotherapy Research*, vol. 21, no. 1, pp. 26–31, 2007.
- [40] D. Ong Lai Teik, X. S. Lee, C. J. Lim, C. M. Low, M. Muslima, and L. Aquili, "Ginseng and ginkgo biloba effects on cognition as modulated by cardiovascular reactivity: a randomised trial," *PLoS One*, vol. 11, no. 3, Article ID e0150447, 2016.
- [41] Y. Z. Wu, S. Q. Li, X. G. Zu, J. Du, and F. Wang, "Ginkgo biloba extract improves coronary artery circulation in patients with coronary artery disease: contribution of plasma nitric oxide and endothelin-1," *Phytotherapy Research*, vol. 22, no. 6, pp. 734–739, 2008.
- [42] H. Zhang, N. Cao, Z. Yang et al., "Bilobalide alleviated dextran sulfate sodium-induced experimental colitis by inhibiting M1 macrophage polarization through the NF- κ B signaling pathway," *Frontiers in Pharmacology*, vol. 11, p. 718, 2020.
- [43] X. Li, L. Huang, G. Liu et al., "Ginkgo diterpene lactones inhibit cerebral ischemia/reperfusion induced inflammatory response in astrocytes via TLR4/NF- κ B pathway in rats," *Journal of Ethnopharmacology*, vol. 249, Article ID 112365, 2020.
- [44] L. Zhang, J. Liu, Y. Ge, and M. Liu, "Ginkgo bilob extract reduces Hippocampus inflammatory responses, improves cardiac functions and depressive behaviors in A heart failure mouse model," *Neuropsychiatric Disease and Treatment*, vol. 15, pp. 3041–3050, 2019.
- [45] O. M. Abdel-Salam, A. R. Baiuomy, S. El-batranM, and S. Arbid, "Evaluation of the anti-inflammatory, antinociceptive and gastric effects of Ginkgo biloba in the rat," *Pharmacological Research*, vol. 49, no. 2, pp. 133–142, 2004.

- [46] I. Ilieva, K. Ohgami, K. Shiratori et al., “The effects of Ginkgo biloba extract on lipopolysaccharide-induced inflammation in vitro and in vivo,” *Experimental Eye Research*, vol. 79, no. 2, pp. 181–187, 2004.
- [47] S. Qian, O. Golubnitschaja, and X. Zhan, “Chronic inflammation: key player and biomarker-set to predict and prevent cancer development and progression based on individualized patient profiles,” *The EPMA Journal*, vol. 10, no. 4, pp. 365–381, 2019.
- [48] B. B. Aggarwal, S. Shishodia, S. K. Sandur, M. K. Pandey, and G. Sethi, “Inflammation and cancer: how hot is the link?” *Biochemical Pharmacology*, vol. 72, no. 11, pp. 1605–1621, 2006.
- [49] G. Sethi, M. K. Shanmugam, L. Ramachandran, A. Kumar, and V. Tergaonkar, “Multifaceted link between cancer and inflammation,” *Bioscience Reports*, vol. 32, pp. 1–15, 2012.
- [50] P. Munkholm, “Review article: the incidence and prevalence of colorectal cancer in inflammatory bowel disease,” *Alimentary Pharmacology & Therapeutics*, vol. 18, no. s2, pp. 1–5, 2003.
- [51] H. Li, X. Xing, X. Zhang et al., “Effects of triptolide on the sphingosine kinase- Sphingosine-1-phosphate signaling pathway in colitis-associated colon cancer,” *International Immunopharmacology*, vol. 88, Article ID 106892, 2020.
- [52] V. S. Kotakadi, Y. Jin, A. B. Hofseth et al., “Ginkgo biloba extract EGb 761 has anti-inflammatory properties and ameliorates colitis in mice by driving effector T cell apoptosis,” *Carcinogenesis*, vol. 29, no. 9, pp. 1799–1806, 2008.
- [53] H. Xu, X. Lyu, M. Yi, W. Zhao, Y. Song, and K. Wu, “Organoid technology and applications in cancer research,” *Journal of Hematology & Oncology*, vol. 11, no. 1, p. 116, 2018.
- [54] T. Režen, D. Rozman, T. Kovács et al., “The role of bile acids in carcinogenesis,” *Cellular and Molecular Life Sciences*, vol. 79, no. 5, p. 243, 2022.
- [55] J. E. Hunt, M. Yassin, J. Olsen, B. Hartmann, J. J. Holst, and H. Kissow, “Intestinal growth in glucagon receptor knockout mice is not associated with the formation of AOM/DSS-Induced tumors,” *Frontiers in Endocrinology*, vol. 12, Article ID 695145, 2021.